

Theoretical investigations of an annular elliptical ring microstrip antenna using Green's function technique

P.Mythili and Annapurna Das

Abstract: Analytical expressions for the Green's function of an annular elliptical ring microstrip antenna (AERMA) are developed and reported. The modal, radiation and input impedance characteristics of the TM_{nm} modes are determined from these expressions. The resonant frequencies of odd modes are greater than that of the even modes for all TM_{n1} modes ($n = 1, 2, 3, \dots$) unlike elliptical microstrip structures. The radiation pattern and input impedance curves of TM_{12} mode on comparison with available experimental result shows good agreement which provides an independent validation to this technique. The performance of the AERMA is then investigated as a function of thickness and substrate dielectric permittivity.

1 Introduction

It is well known that circularly polarised waves may be obtained from circular or square patches using orthogonal feeds [1, 2], elliptical shaped antennas [3] and from elliptical ring structures [4]. Theoretical analysis of an annular elliptical ring microstrip antenna (AERMA) was carried out using generalised transmission line model [4] and mode charts were presented using normalisation technique [5]. A more direct approach i.e. Green's function approach, which is used for other shapes [6–10], has not been applied to AERMA because a computationally efficient Green's function was not available. Although solutions using other approaches were devised for AERMA, they dealt with only the TM_{12} mode [4].

In this paper, expressions for cavity model Green's functions have been derived. The modal field, radiated field and input impedance expressions are developed for a probe-fed confocal AERMA. The radiation characteristics of various TM_{nm} modes are presented and their usefulness are studied. Various losses in the patch and the electric and magnetic energies stored in the fringe regions are taken into account for the analytical expression of the input impedance. The radiation pattern and input impedance for the TM_{12} mode obtained with the present method are compared with the results of [4] and are in good agreement.

2 Cavity model Green's function

A confocal AERMA with dimensions shown in Fig. 1 is considered for the analysis. The Green's function G for this structure is the solution of the wave equation in elliptical coordinates [10] and is expressed as

$$\frac{\partial^2 G}{\partial u^2} + \frac{\partial^2 G}{\partial v^2} + h^2(\cosh 2u - \cos 2v)G = -\delta(u - u_0)\delta(v - v_0) \quad (1)$$

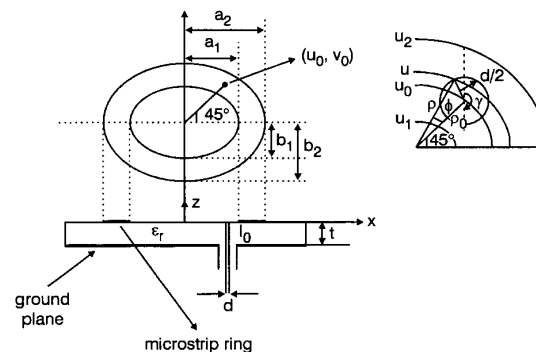


Fig. 1 Geometry of a probe fed AERMA and feed pin

G can be obtained if the complete set of mutually orthogonal eigen function for the given boundary conditions is known. Since the elliptical structure has both odd and even modes, G is a sum of G_o (odd) and G_e (even) modes. Therefore eqn. 1 can be split into two equations.

$$\frac{\partial^2 G_i}{\partial u^2} + \frac{\partial^2 G_i}{\partial v^2} + h^2(\cosh 2u - \cos 2v)G_i = -\frac{\delta(u - u_0)\delta(v - v_0)}{2} \quad (2)$$

$i = e, o$

Initially eqn. 2 with $i = e$ is considered for analysis and G_e is chosen as

$$G_e = \sum_{n=0}^{\infty} \sum_{m=1}^{\infty} \psi_{nme}(u) \text{Se}_n(h_{nme}, \cos v) \quad (3)$$

where $\text{Se}_n(h_{nme}, \cos v)$ is the angular Mathieu function [11] and $h_{nme} = k_{nme}c$ corresponds to even mode cut-off frequency. Substituting eqn. 3 into eqn. 2 and multiplying both sides by $\text{Se}_m(h_{nme}, \cos v)$ and integrating between 0 and 2π , and using the principle of orthogonality we can write

$$-\frac{\partial^2 \psi_{nme}(u)}{\partial u^2} + [b_n^e - h_{nme}^2 \cosh 2u] \psi_{nme}(u) = \frac{\delta(u - u_0) \text{Se}_n(h_{nme}, \cos v_0)}{2M_n^e} \quad (4)$$

© IEE, 1999

IEE Proceedings online no. 19990432

DOI: 10.1049/ip-map:19990432

Paper received 8th September 1998

The authors are with the School of Electronics and Communication Engineering, Anna University, Chennai 600 025, India

where b_n^e is a constant given by

$$b_n^e = \frac{1}{M_n^e} \left[h_{nme}^2 \int_0^{2\pi} \text{Se}_n(h_{nme}, \cos v) \cos 2v dv - \int_0^{2\pi} \frac{\partial^2 \text{Se}_n(h_{nme}, \cos v)}{\partial v^2} \text{Se}_n(h_{nme}, \cos v) dv \right] \quad (5)$$

The solution for the inhomogeneous equation given by eqn. 4 can be found by the method given in [11] and the general solution can be written as

$$\begin{aligned} \psi_{nme}(u) &= \frac{\text{Se}_n(h_{nme}, \cos v_0)}{2M_n^e(h_{nme})(B_n - A_n)} \\ &\times \left(\text{Je}_n(h_{nme}, \cosh u_0) + \frac{B_n}{A_n} \text{Ne}_n(h_{nme}, \cosh u_0) \right) \\ &\times \left(\text{Je}_n(h_{nme}, \cosh u) + \frac{A_n}{B_n} \text{Ne}_n(h_{nme}, \cosh u) \right) \end{aligned} \quad (6)$$

where A_n and B_n are constants. The upper values are for the region $u_1 < u < u_0$ and the lower values are for the region $u_0 < u < u_2$. Therefore from eqns. 3 and 6

$$\begin{aligned} G_e &= \sum_{n=0}^{\infty} \sum_{m=1}^{\infty} \frac{\text{Se}_n(h_{nme}, \cos v_0) \text{Se}_n(h_{nme}, \cos v)}{2M_n^e(h_{nme})(B_n - A_n)} \\ &\times \left[\text{Je}_n(h_{nme}, \cosh u_0) + \frac{B_n}{A_n} \text{Ne}_n(h_{nme}, \cosh u_0) \right] \\ &\times \left[\text{Je}_n(h_{nme}, \cosh u) + \frac{A_n}{B_n} \text{Ne}_n(h_{nme}, \cosh u) \right] \end{aligned} \quad (7)$$

Proceeding through similar steps for $i = o$ from eqn. 2 we get

$$\begin{aligned} G_o &= \sum_{n=0}^{\infty} \sum_{m=1}^{\infty} \frac{\text{So}_n(h_{nmo}, \cos v_0) \text{So}_n(h_{nmo}, \cos v)}{2M_n^o(h_{nmo})(D_n - C_n)} \\ &\times \left[\text{Jo}_n(h_{nmo}, \cosh u_0) + \frac{D_n}{C_n} \text{No}_n(h_{nmo}, \cosh u_0) \right] \\ &\times \left[\text{Jo}_n(h_{nmo}, \cosh u) + \frac{C_n}{D_n} \text{No}_n(h_{nmo}, \cosh u) \right] \end{aligned} \quad (8)$$

where C_n and D_n are constants.

3 Evaluation of constants A_n , B_n , C_n and D_n

Constants A_n , B_n , C_n and D_n are chosen to satisfy the boundary admittance conditions

$$Y_n = -\frac{H_v}{E_z} = \frac{j}{\omega \mu_0 c \sqrt{\cosh^2 u - \cos^2 v}} \frac{\partial E_z}{\partial v} \quad \text{at } u = u_1, u_2 \quad (9)$$

Considering the even mode first

$$\begin{aligned} Y_{ne_{u_2}^{u_1}} &= \frac{j}{kc \sqrt{\cosh^2 u - \cos^2 v}} \\ &\times \frac{\left[\text{Je}'_n(h_{nme}, \cosh \frac{u_1}{u_2}) + \frac{A_n}{B_n} \text{Ne}'_n(h_{nme}, \cosh \frac{u_1}{u_2}) \right]}{\left[\text{Je}_n(h_{nme}, \cosh \frac{u_1}{u_2}) + \frac{A_n}{B_n} \text{Ne}_n(h_{nme}, \cosh \frac{u_1}{u_2}) \right]} \end{aligned} \quad (10)$$

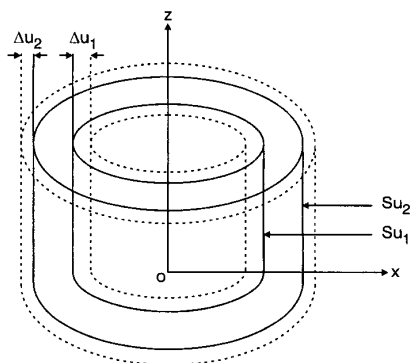


Fig. 2 Equivalent AERMA to find reactive power in the fringe field annular volume

where the prime indicates derivatives with respect to u . The unknown constants are evaluated after finding the boundary admittances. The equivalent boundary admittances at the ring edges make the ring structure an annular cavity with magnetic side walls at the edges and electric walls at the top and bottom. The power flow through the side surfaces Su_1 and Su_2 shown in Fig. 2 can be represented for each mode by

$$\frac{1}{2} \iint_{S_{u_2}^{u_1}} Y_{ne_{u_2}^{u_1}}^* |E_{ze_{u_2}^{u_1}}|^2 ds_{u_2} = P_{re_{u_2}^{u_1}} + jP_{ie_{u_2}^{u_1}} \quad (11)$$

where $E_{ze_{u_1}}$ and $E_{ze_{u_2}}$ are the fringing fields at the edges $u = u_1$ and $u = u_2$, respectively. $P_{re_{u_2}^{u_1}}$ and $P_{ie_{u_2}^{u_1}}$ are the radiated and reactive powers from the respective edges. The normalised Y_n with respect to free space admittance Y_0 leads to

$$y_{ne_{u_2}^{u_1}} = g_{ne_{u_2}^{u_1}} + jb_{ne_{u_2}^{u_1}} \quad (12)$$

and $P_{re_{u_2}^{u_1}}$ and $P_{ie_{u_2}^{u_1}}$ can be found using [9]. The computed $g_{ne_{u_2}^{u_1}}$ and $b_{ne_{u_2}^{u_1}}$ are given by

$$\begin{aligned} b_{ne_{u_2}^{u_1}} &= \frac{\left(\frac{k \varepsilon_r t}{2} \right) \left(\frac{a_1 + b_1}{a_2 + b_2} \right)}{\left(\frac{a_1}{a_2} \right)} \\ &\times \left\{ 1 - \frac{n^2}{k^2 \varepsilon_r \left(\frac{a_1}{a_2} \right)^2} - \frac{1}{\varepsilon_r} |y_{ne_{u_2}^{u_1}} z_0|^2 \right\} \end{aligned} \quad (13)$$

and

$$g_{ne_{u_2}^{u_1}} = \frac{k^2 c^4 \int_0^{2\pi} \int_0^{2\pi} \left\{ \left[\frac{T_1}{T_2} \right]^2 + \cos^2 \theta \left[\frac{P_1}{P_2} \right]^2 \right\} \sin \theta d\theta d\phi}{16t \left(\frac{a_1}{a_2} \right) \pi} \quad (14)$$

where

$$\begin{aligned} T_1 &= \int_{u_1-\delta}^{u_1} \int_0^{2\pi} \text{Se}_n(h_{nme}, \cos v) [\sinh u \cos v \cos \phi \\ &+ \cosh u \sin v \sin \phi] e^{-jk r'} dudv \end{aligned} \quad (15)$$

$$\begin{aligned} P_1 &= \int_{u_1-\delta}^{u_1} \int_0^{2\pi} \text{Se}_n(h_{nme}, \cos v) [\cosh u \cos \phi \sin v \\ &- \sinh u \sin \phi \cos v] e^{-jk r'} dudv \end{aligned} \quad (16)$$

T_2 and P_2 are same as that of T_1 and P_1 but the first integral limit is from u_2 to $u_2 + \delta$ for region 2. Therefore eqn. 12 can be simplified as

$$y_{ne}^{u_1} z_0 = g_{ne}^{u_2} + j \left(\frac{k \epsilon_r t}{2} \right) \left(\frac{a_1 + b_1}{a_2 + b_2} \right) \times \left\{ 1 - \frac{n^2}{k^2 \epsilon_r \left(\frac{a_1}{a_2} \right)^2} - \frac{1}{\epsilon_r} \left| y_{ne}^{u_2} z_0 \right|^2 \right\} \quad (17)$$

Constants A_n and B_n are found by finding the roots of the above quadratic equation and comparing with eqn. 10. Proceeding in a similar way for the odd modes, constants C_n and D_n are also found.

4 Modal field distributions

The AERMA shown in Fig. 1 is excited by a line current I_0 along z -direction by a coaxial feed located at $(u_0, 45^\circ)$ to produce circular polarisation. The current source, assumed to be uniform ($t \ll \lambda_0$), along z due to the probe can be expressed as

$$\vec{J} = \hat{z} I_0 \delta(u - u_0) \quad 0 < z < t \quad (18)$$

Hence the modal fields will have no z variation. The only non-zero components are E_z , H_u and H_v . The eigen value equations of the ring resonator takes the form

$$\frac{J e'_n(h_{nme}, \cosh u_1)}{N e'_n(h_{nme}, \cosh u_1)} = \frac{J e'_n(h_{nme}, \cosh u_2)}{N e'_n(h_{nme}, \cosh u_2)} \quad (19)$$

On solving the above and the corresponding odd mode eigen value equations, the corresponding resonant frequencies are obtained. The electric field inside the cavity is then represented by the equation

$$E_z = j \omega \mu_0 I_0 (G_o + G_e) \quad (20)$$

5 Evaluation of radiated fields

The computation of radiation field at any point (r, θ, ϕ) in the upper half plane $z > 0$ is based on the Fourier transform given by [12] of the aperture fields E_a in the plane $z = 0$. Since the resonator surface at $z = 0$ is assumed to be perfectly conducting, the contribution to the radiation field originates from the fringing fields at the patch edges. Assuming that the fringing fields extend uniformly up to a distance t from the edges and zero beyond that [13], we have $|E_a| = E_{u|u=u_1, u_2} = E_{z|z=u_1, u_2}$ in the two apertures defined by $u_1 - \delta < u < u_1$ and $u_2 < u < u_2 + \delta$, where t in x, y coordinates is equal to δ in u, v coordinate system.

$$\vec{E}_a = \hat{x} E_x + \hat{y} E_y \quad (21)$$

where $E_x = E_z \sinh u' \cos v'$ and $E_y = E_z \cosh u' \sin v'$. The (x, y) components of the Fourier transforms are obtained as

$$f_x = j \omega \mu_0 I_0 \int \int_{app} c^2 \left[\psi_{nme}(u') \text{Se}_n(h_{nme}, \cos v') + \psi_{nmo}(u') \text{So}_n(h_{nmo}, \cos v') \right] \times \sinh u' \cos v' e^{-jk r'} du' dv' \quad (22)$$

$$f_y = j \omega \mu_0 I_0 \int \int_{app} c^2 \left[\psi_{nme}(u') \text{Se}_n(h_{nme}, \cos v') \right]$$

$$\left. \begin{aligned} &+ \psi_{nmo}(u') \text{So}_n(h_{nmo}, \cos v') \right] \\ &\times \cosh u' \sin v' e^{-jk r'} du' dv' \quad (23) \end{aligned}$$

where $r' = x' \sin \theta \cos \phi + y' \sin \theta \sin \phi$.

Radiated fields will add up when aperture field distributions at $u = u_1$ and u_2 are both polarised in the same direction. This means that E_z in the ring structure must alter its polarisation [13]. The radiated fields are computed from the Fourier transforms computed using the equations given in [12].

6 Input impedance

The input impedance seen by the coaxial feed Z_{in} is determined by the conservation of energy principle i.e. by equating the power input to the feed pin with the total power loss

$$Z_{in} = \frac{2}{I_0 I_0^*} (P_f + P_c + P_d) \quad (24)$$

where P_f , P_c and P_d are power losses on feed pin, conductor and the ground plane and the imperfect dielectric substrate, respectively. Feed pin loss is computed using the procedure given by [9]. The feed pin geometry is shown in Fig. 1. For $d \ll \rho_0$ in cylindrical coordinate system

$$\phi \cong -\frac{d \cos \gamma}{2 \rho_0} \quad \text{and} \quad \rho = \rho_0 + \frac{d \sin \gamma}{2} \quad (25)$$

The corresponding parameter in elliptical coordinate system is given by

$$\rho = c \sqrt{\cosh^2 u_0 - \cos^2 v_0} + \frac{d \sin \gamma}{2} \quad (26)$$

Also

$$\rho = c \sqrt{\cosh^2 u - \cos^2 v} \quad (27)$$

Using eqns. 25–27 u and v corresponding to ρ and ϕ are computed. The above transformation is applied to [9] and P_f is written as

$$P_f = \frac{-j \omega \mu_0 t I_0^2}{4 \pi} \int_0^{2\pi} \sum_{n=1}^{\infty} \left[\psi_{ne}(u) \text{Se}_n(h_{nme}, \cos v) + \psi_{no}(u) \text{So}_n(h_{nmo}, \cos v) \right] d\gamma \quad (28)$$

Conductor loss P_c in the ring strip is computed as [1]

$$P_c = \frac{R_s}{\omega^2 \mu_0^2} \int_{u_1}^{u_2} \int_0^{2\pi} \left(\left| \frac{\partial E_z}{\partial u} \right|^2 + \left| \frac{\partial E_z}{\partial v} \right|^2 \right) dudv \quad (29)$$

where $R_s = \sqrt{\omega \mu_0} / 8 \sigma$ and σ is the conductivity of elliptical ring patch conductor. The dielectric loss P_d can be determined by integrating the E field inside the cavity over the cavity volume [1] and is expressed as

$$P_d = \frac{\omega \epsilon_0 \epsilon_r \tan \delta}{2} \times \int_0^t \int_{u_1}^{u_2} \int_0^{2\pi} |E_z|^2 c^2 (\cosh^2 u - \cos^2 v) dt dudv \quad (30)$$

Substituting eqns. 28–30 in eqn. 24 the value of Z_{in} can be calculated.

7 Results and discussion

An AERMA with dimensions $a_1 = 1.45\text{cm}$, $b_1 = 1.34\text{cm}$, $a_2 = 4\text{cm}$, $b_2 = 3.96\text{cm}$, $t = 0.159\text{cm}$ and $\epsilon_r = 2.55$ is considered. The feed is placed at 2 cm from the centre at an angle of 45° with respect to the x -axis. The resonant frequencies for various TM_{nm} modes are computed using eqn. 19 and are given in Table 1 and it is seen that the resonant frequencies for the odd modes are higher than that of the even modes for TM_{n1} modes and the reverse for the modes with $m \neq 1$.

Table 1: Resonant frequencies of an AERMA

Modes	Resonant frequencies	
	odd (GHz)	even (GHz)
TM_{11}	1.151	1.123
TM_{12}	3.820	3.940
TM_{13}	7.449	7.694
TM_{21}	2.169	2.145
TM_{22}	4.634	4.711
TM_{23}	7.818	7.985
TM_{31}	3.107	3.083
TM_{32}	5.534	5.630
TM_{33}	8.325	8.470

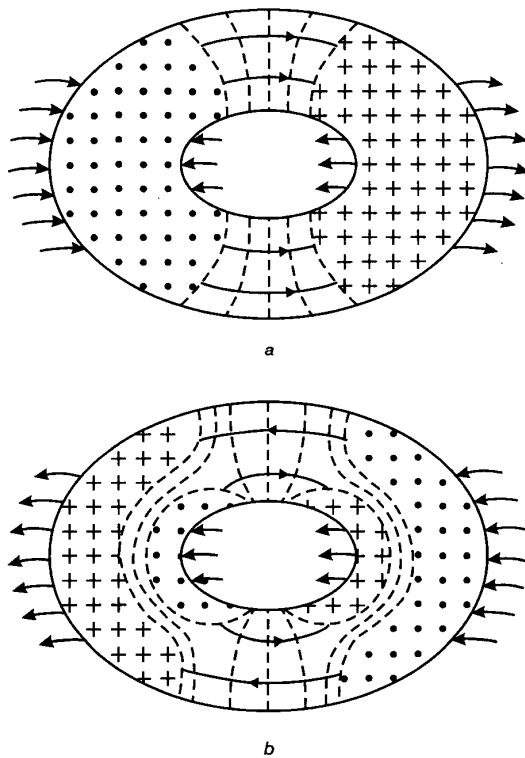


Fig. 3 Field patterns of elliptical ring resonator even modes
 q TM_{11} b TM_{12}
 $J_s = \text{---}\blacktriangle\text{---}$
 $H = \text{---}$
 $E_z = \text{+++}$

Modal field patterns and current distributions on the AERMA for various TM_{nm} even modes are shown in Figs. 3a, 3b, 4a, 4b and 5. The modal field patterns for the TM_{nm} odd modes can be obtained by rotating the corresponding even modes by $\pi/2n$ degrees in the anticlockwise

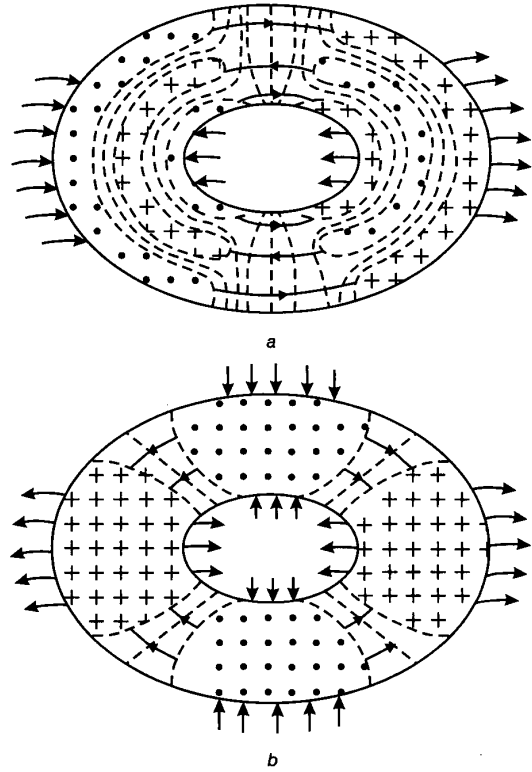


Fig. 4 Field patterns of elliptical ring resonator even modes
 q TM_{13} b TM_{21}
 $J_s = \text{---}\blacktriangle\text{---}$
 $H = \text{---}$
 $E_z = \text{+++}$

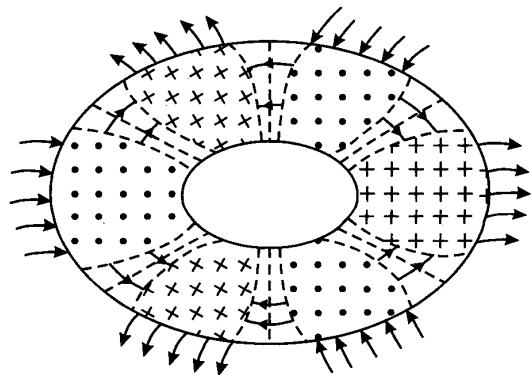


Fig. 5 Field patterns of elliptical ring resonator even modes
 TM_{31}
 $J_s = \text{---}\blacktriangle\text{---}$
 $H = \text{---}$
 $E_z = \text{+++}$

direction. From these modal field patterns, we can observe that the far fields get added when the fringing fields at the inner and outer edges are pointing in the same direction, giving rise to a maximum amplitude in the boresight direction and get subtracted otherwise, giving rise to a null field in the boresight direction. The radiation patterns of various modes are studied out of which a few are shown in Figs. 6a, 6b, 7a and 7b. The radiated fields for all the modes are normalised with respect to the E_0 component of the TM_{12} mode in the $\phi = \pi/2$ plane. The TM_{1m} modes show maximum radiation in the boresight direction. TM_{12} mode is the only mode which gives maximum amplitude radiation at the centre with two small side lobes (Fig. 4b) and is in good agreement with the results of [4]. The modes

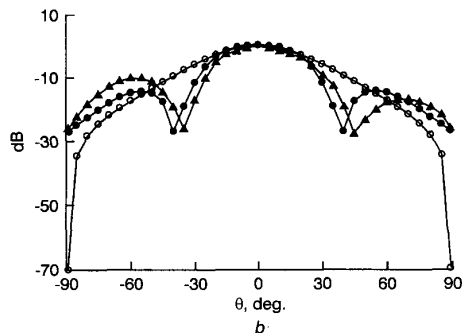
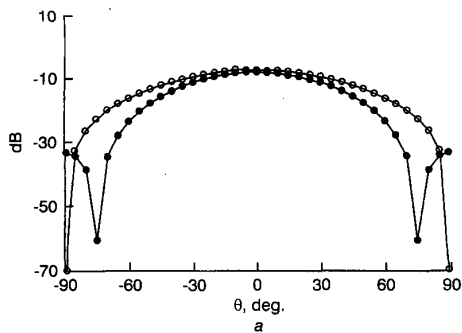


Fig. 6 Radiation patterns of an annular elliptical ring microstrip antenna

a TM_{11}
 E_θ (filled circle)
 E_ϕ (open circle)
 b TM_{12}
 E_θ (filled circle)
 E_ϕ (open circle)
 results of [4] (filled triangle)

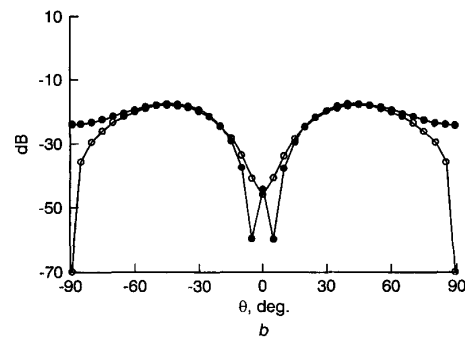
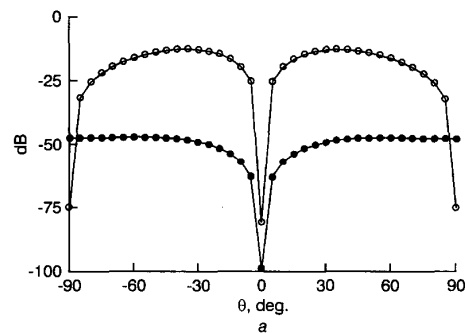


Fig. 7 Radiation patterns of an annular elliptical ring microstrip antenna

a TM_{21}
 E_θ (filled circle)
 E_ϕ (open circle)
 b TM_{31}
 E_θ (filled circle)
 E_ϕ (open circle)

with n even and $m = 1, 2, 3, \dots$ show a deep null at the centre as expected. The modes with $n = 3$ and $m = 1, 2, 3$ have poor radiation in the boresight direction because of the

destructive interference of the fringing fields. Figs. 8 and 9 show the effect of substrate dielectric permittivity and thickness on the radiation pattern of the TM_{12} mode, respectively. It can be seen that as ϵ_r decreases, the radiation amplitude of the main lobe as well as side lobe increases and hence beam width becomes narrower. As substrate thickness t decreases, the amplitude of the main lobe of the radiation pattern as well as the side lobes increases and hence radiation pattern becomes narrower as the nulls shift towards the centre. Therefore it is interesting to note that a reduction in substrate dielectric permittivity or thickness or both should be employed for narrow band applications. The input impedance of the patch has been computed for the dominant TM_{12} mode and is compared with available experimental data [4] as shown in Fig. 10 and a good agreement has been found, which validates well the present model.

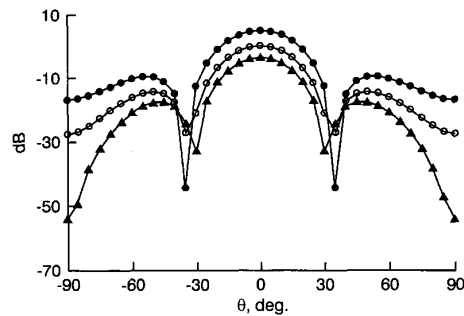


Fig. 8 Effects of substrate dielectric permittivity on the radiation pattern of TM_{12} mode

▲ $\epsilon_r = 2.75$
 ● $\epsilon_r = 2.35$
 ○ $\epsilon_r = 2.55$

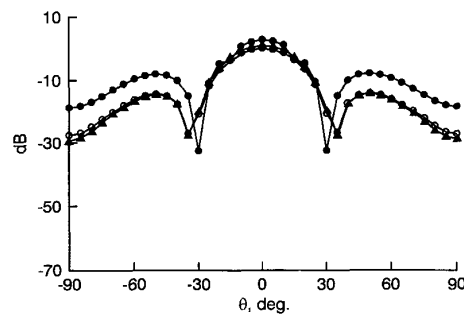


Fig. 9 Effects of substrate thickness on the radiation pattern of the TM_{12} mode

● $t = 0.00039\text{m}$
 ○ $t = 0.00159\text{m}$
 ▲ $t = 0.00259\text{m}$

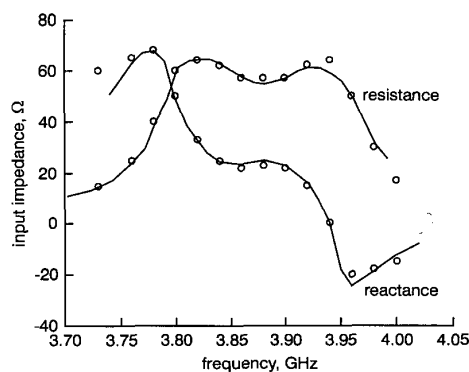


Fig. 10 Comparison of theoretical and experimental input impedance curves for the TM_{12} mode

○ experimental, — theoretical

8 Conclusion

Analytical expressions for the cavity model Green's function of a confocal annular elliptical ring microstrip antenna have been derived. Modal, radiated fields and input impedance of various modes are computed using these expressions. A reduction in the substrate dielectric permittivity or the substrate thickness should be employed for narrow band applications.

9 References

- 1 BHAL, I.J., and BHARTIA, P.: 'Microstrip antennas' (Artech House, Dedham Massachusetts, 1980)
- 2 CARVER, K.R., and MINK, J.W.: 'Microstrip antenna technology', *IEEE Trans. Antennas Propag.*, 1981, **AP-29**, pp. 2-24
- 3 SHEN, L.C.: 'The elliptical microstrip antenna with circular polarization', *IEEE Trans. Antennas Propag.*, 1981, **AP-29**, pp. 90-94
- 4 BHATTACHARYYA, A.K., and SHAFAI, L.: 'Theoretical and experimental investigation of the elliptical annular ring antenna', *IEEE Trans. Antennas Propag.*, 1988, **36**, pp. 1526-1530
- 5 ALHARGAN, F.A., and JUDAH, S.R.: 'Mode charts for confocal annular elliptic resonators', *IEE Proc.-H*, 1996, **143**, pp. 358-360
- 6 OKOSHI, T., and MIYOSHI, T.: 'The planar circuit - An approach to microwave integrated circuitry', *IEEE Trans. Microw. Theory Tech.*, 1972, **MITT-20**, pp. 245-252
- 7 OKOSHI, T., TAKENCHI, T., and HSU, J.P.: 'Planar 3-D hybrid circuit', *Electron. Commun. (Japan)*, 1975, **58-B**, pp. 80-90
- 8 CHADHA, R., and GUPTA, K.C.: 'Green's functions for triangular segments in planar microwave circuits', *IEEE Trans. Microw. Theory Tech.*, 1980, **MITT-28**, pp. 1139-1143
- 9 DAS, A., and DAS, S.K.: 'Input impedance of a probe excited circular microstrip ring antenna', *IEE Proc.-H*, 1985, **132**, pp. 384-390
- 10 ALHARGAN, F.A., and JUDAH, S.R.: 'A general mode theory for the elliptical disk microstrip antenna', *IEEE Trans. Antennas Propag.*, 1995, **43**, pp. 560-568
- 11 MORSE, P.M., and FESHBACH, H.: 'Methods of theoretical physics' (McGraw Hill, New York, 1953)
- 12 COLLIN, R.E., and ZUCKER, F.J.: 'Antenna theory Pt. 1' (McGraw Hill, New York, 1969)
- 13 DAS, A., DAS, S.K., and MATHUR, S.P.: 'Radiation characteristics of higher order modes in microstrip ring antenna', *IEE Proc.-H*, 1984, **131**, pp. 102-106